Heliyon 10 (2024) e39571

Contents lists available at ScienceDirect

Heliyon

journal homepage: www.cell.com/heliyon

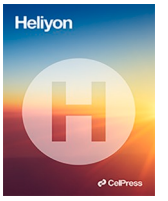

Research article

Pharmacological inhibition of PLK2 kinase activity mitigates cognitive decline but aggravates APP pathology in a sex-dependent manner in APP/PS1 mouse model of Alzheimer's disease

Laura Martínez-Drudis [a,b], Morgan Bérard [a,b], Dylan Musiol [a,b], Serge Rivest [a,b], Abid Oueslati [a,b,*]

[a] CHU de Québec-Université Laval Research Center, Neuroscience Axis, 2705 Boulevard Laurier, Quebec City, Canada
[b] Department of Molecular Medicine, Faculty of Medicine, Université Laval, Quebec City, Canada

ARTICLE INFO

Keywords:
Polo-like kinase 2
Alzheimer's disease
Sex dimorphism
Amyloid β
APP/PS1 mouse model

ABSTRACT

Converging evidence from clinical and experimental studies suggest the potential significance of Polo-like kinase 2 (PLK2) in regulating the phosphorylation and toxicity of the Alzheimer's disease (AD)-related protein, amyloid precursor protein (APP). These findings have prompted various experimental trials aimed at inhibiting PLK2 kinase activity in different transgenic mouse models of AD. While positive impacts on cognitive decline were reported in these studies, the cellular effects remained controversial. In the present study, we sought to assess the cognitive and cellular consequences of chronic PLK2 inhibitor treatment in the APP/PS1 transgenic mouse model of AD. First, we confirmed that inhibiting PLK2 prevented cognitive decline in a sex-dependent manner, particularly by enhancing working memory in male APP/PS1 mice. Surprisingly, cellular analysis revealed that treatment with PLK2 inhibitor increased the load of amyloid plaques and elevated levels of soluble amyloid β (Aβ) 40 and Aβ42 in the cortex, as well as insoluble Aβ42 in the hippocampus of female mice, without affecting APP pathology in males. These results underscore the potential of PLK2 inhibition to mitigate cognitive symptoms in males. However, paradoxically, it intensifies amyloid pathology in females by enhancing APP amyloidogenic processing, creating a controversial aspect to its therapeutic impact. Overall, these data highlight the sex-dependent nature of the effects of PLK2 inhibition, which may also be influenced by the genetic background of the transgenic mouse model utilized.

1. Introduction

Alzheimer's disease (AD), the most common cause of dementia, is estimated to affect more than 55 million people worldwide [1,2]. This progressive neurodegenerative disorder, characterized by memory impairment and cognitive decline, is in part instigated by the aberrant accumulation of amyloid β (Aβ), a peptide derived from the sequential cleavage of the amyloid precursor protein (APP) by β- and γ-secretases [1,3–5]. Aβ deposits are the main component of amyloid plaques, one of the main neuropathological hallmarks of AD

* Corresponding author. CHU de Québec-Université Laval Research Center and Department of Molecular Medicine, 2705, boulevard Laurier, G1V 4G2, Quebec City, Canada.
E-mail address: abid.oueslati.1@ulaval.ca (A. Oueslati).

https://doi.org/10.1016/j.heliyon.2024.e39571
Received 22 August 2024; Received in revised form 16 October 2024; Accepted 17 October 2024
Available online 18 October 2024

[3,6–8]. Mutations in the genes coding for APP and presenilin 1 and 2 (PS1/2), the catalytic subunits of the γ-secretase complex, enhance the production and aggregation of Aβ, and are associated with early onset familial AD (FAD) [9–13]. Moreover, several studies have demonstrated that animal models injected with Aβ oligomers or overexpressing FAD mutated genes present with neuronal dysfunction and cognitive deficits [14–20]. These observations suggest that APP amyloidogenic cleavage and the subsequent Aβ production and accumulation represent a major pathological pathway in AD. Therefore, identifying the molecular components involved in regulating APP processing could aid in the development of disease-modifying therapies for AD.

Converging lines of evidence from clinical and experimental studies suggest that post-translational modifications (PTMs), and particularly phosphorylation, can regulate the fate of APP [21,22]. Recently, Polo-like kinase 2 (PLK2) has been identified as one of the key kinases involved in APP phosphorylation, and as a new player in AD pathogenesis [23–25]. Indeed, studies have reported elevated levels of this serine/threonine (S/T) kinase in the brain of patients and animal models of AD [25–27], in addition to an association between PLK2 polymorphisms and AD risk [28]. Moreover, our team and others have reported that PLK2 activity-dependent phosphorylation of APP at threonine 668 (T668) decreases full-length APP protein levels in cell culture, possibly by increasing its amyloidogenic processing [23,24]. These observations suggested that modulating the activity of PLK2 may have a potential therapeutic application for the treatment of AD. Although a beneficial effect of PLK2 inhibition on the cognitive symptoms has been reported *in vivo*, in transgenic mouse models of AD, the effect of this treatment on Aβ pathology led to controversial results. While Lee and colleagues reported that treatment with the pan-specific PLK inhibitor, volasertib (BI6727), lowered Aβ formation and accumulation in 5XFAD transgenic mice [25]. In contrast, our recent study showed that treatment with a selective PLK2 inhibitor, PLK2i #37, did not affect Aβ pathology, but rather reduced Tau burden, in a sex-dependent manner, in 3xTg-AD mouse model of AD [23], a model presenting Aβ and Tau pathologies [29,30]. These observations imply that, beyond the influence of sex, the outcomes of inhibiting PLK2 activity may be contingent upon the specific attributes of the transgenic models of AD that are employed. Of note, transgenic models of AD with different genetic backgrounds and modifications exhibit unique disease onset and progression patterns [20,31–38]. This implies that the response to approaches targeting the reduction of APP phosphorylation by inhibiting PLK2 activity may also be influenced by the genetic background.

To validate this hypothesis, in the present study, we investigated the impact of PLK2 pharmacological inhibition, using a potent, highly selective, and brain-penetrant inhibitor, PLK2i #37 [39–41], on Aβ pathology and AD-like symptoms in a transgenic mouse model of AD with a pure Aβ pathology, namely APP/PS1 mice [42,43]. Our results revealed a sex-specific effect of the treatment at both the molecular and behavioral levels. Indeed, chronic treatment with PLK2i #37 prevented working memory impairment in male APP/PS1 mice, while both Aβ accumulation and synaptic protein expression levels remained unchanged by the treatment. In contrast, amyloidogenic pathology was increased in treated APP/PS1 females. Collectively, our data support the therapeutic potential of PLK2 pharmacological inhibition for the treatment of AD. Moreover, our study underscores the significance of considering not only sex-dependent effects, but also genetic context when using animal models to assess AD therapeutics.

2. Materials and methods

2.1. Treatment with PLK2 pharmacological inhibitor

Animals were housed at a constant temperature (~22 °C) and under a 12 h light/dark cycle, with free access to food and water [23]. APP/PS1 mice (B6; C3-Tg (APPswe, PSEN1dE9) 85Dbo/Mmjax) were acquired from The Jackson Laboratory and maintained on a C57BL/6J background in an in-house colony at the CHU de Québec-Université Laval Research Center. This transgenic mouse model of Aβ pathology expresses both mouse and human APP695 harboring the double Swedish mutation (K595N/M596L) and the mutant human presenilin-1 (exon 9 deletion (dE9) variant) genes under the control of the mouse prion protein promoter [42,43].

Three-month-old (±1 week) APP/PS1 mice underwent a regimen of daily intraperitoneal administration of PLK2i #37 [39] at a concentration of 10 mg/kg (APP/PS1 PLK2i #37, n = 8–10 per sex) for 4 months. Control age- and sex-matched WT and APP/PS1 littermates received injections of 0.9 % NaCl solution (WT Saline, n = 13 per sex; APP/PS1 Saline, n = 9–13 per sex). The treatment assigned to each APP/PS1 mouse was randomized.

2.2. Behavioral analysis

Five different behavioral tests were performed during the last month of treatment. All behavioral tests were performed in the morning, after receiving the daily treatment by a different experimenter, as previously described [23]. Three days before the first test, mice underwent a 4 h-habituation to the testing room. Before each test, animals were allowed to acclimate to the room for 30 min. 70 % ethanol was used to clean the arenas between animals for all tests, except for the water maze. ANY-maze video tracking software (Version 4.8; Stoelting Co., Wood Dale, Il) was used for all the tests, except for the open field. The experimenter was out of view for all the tests.

2.2.1. Elevated plus maze test

Anxiety-like behavior was evaluated using the elevated plus maze (EPM) [44,45]. The apparatus, constructed from beige Plexiglass, featured two opposite enclosed arms (15 cm-high walls) and two opposite open arms (no walls), 5 cm wide and 30 cm long each, and raised 40 cm above the base. Mice were placed at the intersection between the four arms (maze center) facing the open arms for 5 min. An animal was considered inside a zone whenever its center point (body's middle) was within it. The experimenter scored the time spent and the number of entries in each arm.

2.2.2. Open field test

The open field (OF) test was performed in a photobeam activation system (PAS) arena, as previously described [46]. The distance traveled was retrieved from the PAS software in 5-min bins and used to evaluate locomotor activity (distance traveled during the first 10 min of the test) and intrasession habituation (activity change ratio calculated as distance traveled during the last 5 min divided by the sum of the distances traveled during the first 5 min and the last 5 min) [47–49].

2.2.3. Spontaneous alternation (Y-maze) task

Spatial working memory was evaluated by the spontaneous alteration test [50,51] using a symmetrical Y-maze with three identical equal-sized arms, as previously described [52]. To prevent animals from relying on visual or spatial cues, the arms of the apparatus were covered with black laminated paper, while the bottom was covered by white laminated paper to provide better contrast [52]. Mice were placed at the intersection between the three arms (maze center) for 5 min. The sequence and number of entries to the different arms were recorded by the experimenter, with an entry counted only when the animal had fully entered the corresponding arm. Data were analyzed based on the percentage of correct alternations, as previously described [52].

2.2.4. Morris water maze test

Spatial learning and memory as well as cognitive flexibility were evaluated using the Morris water maze (MWM) task by training the animals to find the location of an escape platform (reinforcement) [53–55]. The MWM apparatus consisted of a circular pool (40 cm height and 78 cm diameter) made of clear acrylic and divided into four quadrants (N, S, E, and W). An escape platform (9 cm diameter and 15 cm height) was submerged at the center of the target quadrant, 1–2 cm under the water surface [56]. The water was kept at 25 °C (±0.5 °C) and made opaque with powder milk to hide the platform. Four extra-maze clues, one for each quadrant, were affixed to the outer walls of the pool to provide spatial configuration and allow for the identification of the target quadrant containing the hidden platform. The spatial clues had different colors, shapes, and dimensions, and along with all other visual stimuli in the room, remained constant during the entire experiment.

The test was performed over ten consecutive days and divided into an acquisition phase and a reversal phase, both followed by a probe trial. During the acquisition and the reversal phases, consisting of 4 consecutive days each (acquisition: days 1–4, reversal: days 5–9), mice underwent four trials per day every 30–60 min. For each trial, mice were positioned along the edge of the pool with their heads directed towards the wall of the pool at one of the quadrants' intersections (NE, NW, SW, and SE). The starting intersection was randomly altered between trials and was never repeated within the same day. Mice had 60 s per trial to find the platform. The test ended when the animal reached the platform, where it remained for 5 s. If the animal failed to reach the platform within 60 s, it was gently guided to it and allowed to stay there for 15 s. After each trial, the mice were dried and given time to rest in their home cage between trials. The location of the platform (target quadrant: E) was maintained during the four acquisition days. For the reversal phase, the platform was placed on the opposite quadrant (W) to test the animals' cognitive flexibility [53]. One day after both the acquisition and the reversal phase (days 5 and 10), retention of the task was assessed by a probe trial [47,53–55], consisting of a 60-s free swim in the absence of the platform. For the probe trials, mice were positioned at the cardinal point opposite to the platform's location from the previous day (acquisition: W, reversal: E). For the acquisition and reversal trials, the latency and distance traveled to reach the platform were recorded. For each parameter, the average from the four trials was calculated per training day. For the probe trial, the time and distance swam in each quadrant were recorded. Reaching the platform for at least half the trials was necessary to be included in the analysis.

2.2.5. Social approach test

The animals' social behavior was evaluated using Crawley's social approach test [57–59]. Three days prior to the testing (at the end of the MWM reversal probe trial), mice were separated and individually housed for the remainder of the protocol. The test was performed in an apparatus with three compartments made of clear Plexiglas. Each compartment measured 40 cm in length, 20 cm in width, and 22 cm in height. Each lateral compartment (left and right) was separated from the central compartment by a wall presenting a door on its center (an opening of 6 cm in width and 8 cm in height) and contained a metal mesh cup (container of 9 cm in diameter and 10 cm in height placed in the center, 5 cm from the compartment's lateral wall) that permitted visual, olfactory, and auditory interaction. The test consisted of two sessions: habituation and social interaction. For each session, mice were placed in the central compartment and were allowed to freely explore for 5 min. Between sessions (3-min interval), mice were briefly placed back in their cages. During the habituation session, the experimenter recorded the time spent by the mice in each compartment in real time. In the second session (social interaction), a new mouse with the same age, sex, and genotype as the tested mouse was placed in the container (social container) of the less explored compartment during the habituation session, while the other container remained empty. The time spent by the tested mouse in each compartment and the time that the animal spent exploring each container (social and empty) were recorded by the experimenter. A social preference ratio was determined as follows: time exploring the social container divided by the time exploring both containers.

2.3. Tissue collection and preparation

After the last behavioral test, mice were deeply euthanized with an intraperitoneal injection of ketamine (100 mg/ml) and xylazine (10 mg/ml) (0.1 ml/30 g). Mice were intracardially perfused with ice-cold PBS (0.1 M; pH 7.4) containing phosphatases (50 mM sodium fluoride and 1 mM sodium pyrophosphate) and protease inhibitors (S8820; Sigma-Aldrich, St. Louis, USA). Brains were collected and the two hemispheres were separated. One brain hemisphere was immediately fixed in 4 % PFA for 24 h, then incubated in

4 % PFA and 20 % sucrose for 24 h and processed for immunohistochemistry. The other hemisphere was dissected and kept at −80 °C until processing for biochemical analysis.

2.3.1. Tissue processing for biochemical analysis

The cortex and hippocampus of the frozen hemisphere were micro dissected and homogenized with a tissue homogenizer (Bio-Gen PRO200 Homogenizer; ProScientific, Oxford CT, USA) in 800 μl or 240 μl (eight volumes), respectively, of Radioimmunoprecipitation assay (RIPA) buffer with 1 % protease inhibitor cocktail 100× (B14001; Bimake, Houston, TX, USA) and 1 % phosphatase inhibitor cocktail 100× (B15002; Bimake, Houston, TX, USA). Tissue lysates were then sonicated in ice-cold H_2O (bath sonication; 90 % amplitude; 45 s with 1 s on and 2 s off) (Fisherbrandtm Model 505 sonicator). After sonication, lysates were centrifuged at 13000 rpm at 4 °C for 30 min, generating a detergent-soluble fraction (supernatant).

The residual pellets, considered as the detergent-insoluble fraction, were further homogenized in 600 μl or 160 μl (cortex and hippocampus, respectively) of 5 M guanidine-HCl (in 50 mM Tris-HCl; pH 8) by pipetting up and down. After homogenization, samples were sonicated in an ice-cold H_2O (bath sonication; 90 % amplitude; 45 s with 1s on and 2 s off) (Fisherbrandtm Model 505 sonicator). The samples were then sonicated a second time (same parameters). Next, a portion of each sample was diluted tenfold in cold 0.1 M PBS with 1 % protease inhibitor (B14001; Bimake, Houston, TX, USA), then centrifuged at 16 000 g to generate the insoluble fraction (guanidine extracts, supernatant). Total protein concentration was determined for each fraction (soluble and insoluble) using a Bicinchoninic acid (BCA) Protein Assay Kit (ThermoFisher Scientific, Waltham, MA, USA). After aliquoting, all samples were kept at −80 °C for biochemical analysis.

2.3.2. Tissue processing for immunohistochemistry

Using a frozen microtome (Leica Microsystems, Concord, ON, Canada), the fixed brain tissue was cut into 25 μm-thick coronal sections. These sections were collected serially, preserved in a cryoprotection solution (0.05 M sodium phosphate buffer (pH 7.3), 20 % glycerol, and 30 % ethylene glycol) and stored at −20 °C.

Table 1
List of antibodies used in the present study.

Antigen/Species	Antibody name/Catalog number	Epitope	Concentration Western Blot	Concentration Immunostaining	Source
Primary antibodies					
α-syn pS129 /mouse	Phosphorylated α-synuclein pSyn #64/015–25,191	Phospho-serine 129	200 ng/μL		FUJIFILM Wako Pure Chemical Corporation (Richmond, VA, USA)
α-syn /rabbit	Anti-Alpha-synuclein antibody [MJFR1] /ab13850	118–123	1:1000		Abcam (Cambridge, UK)
Aβ /mouse	β-amyloid clone 6E10/803001	1–16	1:1000	1:1000	Biolegend (San Diego, CA, USA)
APP /mouse	Amyloid precursor protein clone Y188/ab32136	750 to C-terminus	1:2500		Abcam (Cambridge, UK)
APP pT668 /rabbit	Amyloid precursor protein phospho T668 clone EPR7074(N)/ab206297	Phospho-threonine 668	1:1000		Abcam (Cambridge, UK)
Drebrin /mouse	Drebrin clone MX823/612128	C-terminal 632–649 coupled to KLH	1:1000		Progen (Heidelberg, Germany)
GAPDH	GAPDH loading control/G041	–	1:5000 – 1:2500		Abm (Vancouver, BC, Canada)
PSD95 /mouse	PSD95 clone K28/43/75-028	77-299 (PDZ domains 1 and 2)	1:1000		UC Davis /NIH NeuroMab Facility (Davis, CA, USA)
Synapto-physin /rabbit	Synaptophysin/PA1-1043	253–272	1:25000		Invitrogen (Waltham, MA, USA)
Secondary antibodies					
Alexa Fluor 633 anti-mouse (H + L) /goat	Alexa Fluor 633 goat anti-mouse/ A-21052			1:1000	Invitrogen (Waltham, MA, USA)
Mouse IgG (680RD) /goat	IRDye® 680RD- conjugated anti-mouse secondary antibody/ 926–68070		1:10000		LI-COR Biosciences (Lincoln, NE, USA)
Rabbit IgG (800CW) /goat	IRDye® 800CW-conjugated anti-rabbit secondary antibody/ 926–32211		1:10000		LI-COR Biosciences (Lincoln, NE, USA)

2.3.3. Western blot (SDS-PAGE)

For each brain structure (cortex and hippocampus), proteins from the detergent-soluble fraction were diluted in 4× Laemmli buffer (Bio-Rad, Hercules, CA, USA) and incubated at 95 °C for 5 min. Subsequently, 15 μl-samples, containing 20 μg of proteins, were separated in a 8–16 % Tris-Glycine gel (Bio-Rad, Hercules, CA, USA) for the analysis of synaptic proteins, and a 4–20 % Tris-Glycine gel (Bio-Rad, Hercules, CA, USA) for the detection of APP and its C-terminal fragments (CTFs). After gel electrophoresis (100–180 V), wet transfer (90 V for 90 min) or the Trans-Blot Turbo Transfer system (Bio-Rad, Hercules, CA, USA) were used to transfer proteins into nitrocellulose membranes. For α-synuclein, samples were loaded on a 12 % SDS-Polyacrylamide gel electrophoresis (PAGE) gel, ran at 60–90 V, and transferred into a nitrocellulose membrane using wet transfer on ice (at 200–350 mA). The membranes were then heated in 0.1 M PBS to enhance epitope exposure, followed by an incubation with blocking solution (0.1 M PBS-0.1 % Tween (PBS-T) with 3 % gelatin from coldwater fish) for 1 h at room temperature (RT). Afterward, the membranes were either incubated for 2 h at RT or overnight (ON) at 4 °C with primary antibodies (Table 1). After three washes in PBS-T, membranes were incubated with appropriate secondary antibodies (Table 1). Finally, membranes were scanned using the LI-COR Odyssey scanner (LI-COR Lincoln, NE, USA). Protein levels were normalized using Glyceraldehyde 3-phosphate dehydrogenase (GAPDH) or the corresponding total protein for phosphorylated forms. The obtained ratios were then normalized to WT Saline group for synaptic markers, or to APP/PS1 Saline group for human APP and its cleavage products, and α-synuclein.

2.3.4. Enzyme-linked immunosorbent assay (ELISA)

Aβ40 and Aβ42 levels were evaluated in both the soluble and insoluble fractions of APP/PS1 mice for each brain structure (hemi-cortex and hemi-hippocampus) using a human Aβ ELISA kit (KHB3481 and KHB3544; Invitrogen, Waltham, MA, USA). Samples from a male and a female WT mice were used as negative controls. All samples were diluted in standard diluent buffer as follows: 1:15 (Aβ40) or 1:30 (Aβ42) for the detergent-soluble fraction and 1:100 (Aβ40) or 1:1500 (Aβ42) for the insoluble fraction (guanidine extracts). Aβ peptide standards were diluted in standard diluted buffer with the corresponding extraction buffer (RIPA or guanidine-HCl) at the corresponding dilution to maintain the same composition of buffers used for the diluted experimental samples. Briefly, 50 μl of standards and samples were dispensed in pre-coated plates containing anti-Aβ40 or anti-Aβ42 antibodies together with 50 μl of human Aβ40 or Aβ42 detection antibody solution, respectively, and incubated at RT for 3 h. Next, samples were washed four times with 1× wash buffer and incubated with 100 μl of horse peroxidase (HRP)-conjugated anti-rabbit IgG antibody at RT for 30 min, followed by four additional washes. HRP reaction was catalyzed using 3,3′,5,5′-Tetramethylbenzidinesolution (30 min incubation at RT with 100 μl of stabilized chromogen, protected from light). Finally, the reaction was terminated with 100 μl of Stop solution, and absorbance was measured at 450 nm using a Synergy HT microplate reader (BioTek, Winooski, VT). A 4-parameter algorithm was used to generate the standard curve and determine the levels of Aβ40 and Aβ42 peptides, and then normalized to the total protein for each sample.

2.3.5. Immunofluorescence and quantification of amyloid plaques

Free-floating hippocampal sections were rinsed three times with PBS for 10 min and blocked for 2 h at RT in PBS-0.3 % Triton X-100 with 5 % normal goat serum (NGS) and 1 % bovine serum albumin (BSA). Sections were then incubated at 4 °C ON with primary antibodies (1:1000) (see Table 1) in PBS-0.1 % Triton X-100 with 3 % NGS and 1 % BSA, followed by an incubation with the corresponding secondary antibody for 2 h at RT (see Table 1). Finally, nuclear staining was performed by incubating tissue sections in 4′,6-diamidino-2-phenylindole (DAPI) (1:10000) for 7 min at RT. Afterward, sections were serially mounted on glass slides in Fluoromount-G mounting media (17984–25; EMS, Hatfield, PA, USA) for microscopy imaging.

Images of the entire hemisphere were captured using epifluorescence Axio Observer microscope. Evaluation of the number and the size of Aβ plaques in the cortex and the hippocampus were performed in a blinded manner by analyzing every twelfth serial coronal section covering the entire hippocampus (5–7 sections per animal for the cortex, 4 to 5 sections per animal for the dorsal hippocampus; 25 μm in thickness). Briefly, the regions of interest were delineated (full surface of the cortex and full surface of the dorsal hippocampus), and the contour of 6E10-positive plaques was traced using the Neurolucida software (Microbrightfield, Williston, VT, USA). The number of plaques was adjusted to the total surface of the corresponding analyzed brain structure. The size of the plaques was calculated by averaging the plaque surfaces per animal.

2.4. Experimental blinding

Blinding procedures were applied in this study. During the behavioral testing phase, treatments to animals were administered by an independent experimenter. This experimenter was responsible for assigning a unique code to each animal, obscuring the animals with respect to their genotype and the specific treatment they received. This protocol ensured that the experimenter responsible for conducting the behavioral testing and analysis remained blinded to these variables.

A similar blinding approach was applied for immunohistological analysis. The application of unique codes to each animal during the imaging and quantification of amyloid plaques was used to maintain the blindness of the experimenter to the experimental group of the animals for this phase of the study.

Following the completion of data collection, the unique codes were decoded, and statistical analysis and graphical representation of the results were performed.

2.5. Statistical analysis

Outliers, identified as values that exceeded the 1.5 interquartile ranges below the first quartile or 1.5 interquartile ranges above the

third quartile, were excluded from the analysis on a test-by-test basis. We used Student's unpaired two-sample t-tests to compare the two groups (Saline and PLK2i#37). We also used one-way ANOVA followed by Tukey's multiple comparisons test to compare one independent variable between the three experimental groups (WT Saline, APP/PS1 Saline, and APP/PS1 PLK2i#37). We used two-way ANOVA followed by Sidak's multiple comparisons tests to compare differences between males and females for each experimental group. We used one sample t-tests to evaluate if habituation, spontaneous alternation, and social preference ratios obtained in the OF, the Y-maze, and the social approach tests, respectively, were significantly different from 50 % for each experimental group. To evaluate differences between groups over time and within each group over time during the acquisition and reversal phases of the MWM task, a two-way repeated measures ANOVA was performed, followed by Tukey's or Dunnett's multiple comparisons tests. $P < 0.05$ was defined as statistically significant. Data are presented as the means ± standard error of the mean (S.E.M.). We used Prism 8 software (GraphPad software, San Diego, CA, USA) to prepare Graphs and perform statistical analysis.

3. Results

3.1. Chronic treatment with PLK2i #37 reduces cognitive decline in APP/PS1 mice in a sex-specific manner

Puzzled by inconsistent findings in prior research conducted in our laboratory and by others, which reported conflicting results on the cellular impact and the involvement of the Aβ pathway in the positive outcomes of pharmacological inhibition of PLK2 activity in different transgenic mouse models of AD [23,25], we sought to better understand the effect of PLK2 inhibition on Aβ pathology in a pure APP-based transgenic mouse model of AD, namely APP/PS1 mice [42,43]. This model exhibits an age-dependent and region-specific progression of Aβ deposition, starting at the age of 3–4 months, in the frontal cortex and the hippocampus [43,60] (Fig. 1A). Thus, we decided to treat 3-month-old (±1 week) male and female mice with a daily intraperitoneal injection with PLK2i #37 at the concentration of 10 mg/kg or saline for 4 months (Fig. 1A). This experimental paradigm was designed to investigate the impact of chronic administration of PLK2 inhibitor on the disease progression. Of note, the treatment's efficacy was assessed by measuring α-synuclein (α-syn) phosphorylation levels, a well-established PLK2 substrate [26,40,41,61–66]. We observed a decrease of phosphorylated-S129 α-syn (pS129) in the cortex of treated APP/PS1 mice, compared to their non-treated counterparts (Fig. S1), corroborating previous reports [39–41], and supporting the capacity of PLK2i #37 to reduce PLK2 activity in mice brains.

During the last month of treatment, from 6 to 7 months of age, the behavioral performance of the mice was evaluated using multiple behavioral tests to assess the treatment's ability to halt cognitive decline (Fig. 1B). First, we evaluated the animals' anxiety-like behavior, as well as their locomotor and exploratory activities, using the EPM [44,45] and the OF [47,48] tests, respectively [44,45,67]. The EPM test was used to measure the conflict between exploring a new environment and avoiding brightly lit open areas [47]. In this test, APP/PS1 females allocated more time in the open arms (Fig. 1C) while spending less time in the enclosed arms of the maze (Fig. 1D), compared to the performances of WT littermates. This effect was not impacted by PLK2i #37 treatment (Fig. 1C and D). Of note, while no significant differences were observed amongst male groups (Fig. 1C and D), the two-way ANOVA test revealed no effect of sex in this test (Table 2). Similarly, consistent with previous reports [31,68–72], both male and female APP/PS1 mice exhibited increased travel distance in the OF, compared to WT mice (Fig. 1E). This increased locomotor activity was not affected by the treatment with PLK2i #37 (Fig. 1E). Collectively, our results demonstrated that the hyperactivity and behavioral disinhibition displayed by APP/PS1 mice in EPM and OF tests, also found in other AD models and human patients [70,73–78], remained unchanged upon treatment with PLK2i #37.

Moreover, evaluation of the animals' performances in the OF test was also used to test cognition by examining the intrasession habituation during the 1 h trial [49]. All groups, with or without treatment, displayed an activity change ratio significantly lower than 50 % (Fig. 1F), indicating a reduction of exploratory activity over time, hence reflecting a normal short-term memory and habituation behavior.

Next, we used Y-maze spontaneous alternation [50,51] and the MWM [53–55] tests to assess spatial working memory and reference memory. In the Y-maze test, saline-treated APP/PS1 males exhibited working memory deficits, as shown by a reduced percentage of spontaneous alternation when compared to WT mice (Fig. 1G). Interestingly, this deficit was prevented by the treatment with PLK2i #37 (Fig. 1G). Of note, no deficits were observed for the females, all groups scoring above chance level (50 %) (Fig. 1G). Moreover, while the main effect of sex was not significant, multiple comparisons revealed significant differences between males and females for the APP/PS1 Saline group (Table 2).

The MWM task was used to assess spatial learning and memory [53–55]. During the acquisition phase of the test (days 1–4), the distance traveled and latency to reach the platform were significantly reduced over time for all groups when compared to the first day of training (day 1) (Fig. 1H and Fig. S2A), suggesting good spatial learning and memory levels, as previously reported [79,80]. However, while the mean distance did not significantly differ between male groups, a notable difference in overall performance of the mice was observed between APP/PS1 and WT females, when all days were considered (Fig. 1H and Fig. S2A). Supporting these findings, in the probe trial (day 5), although differences between groups and sexes were not significant and two-way ANOVA revealed no effect of sex (Table 2), non-treated APP/PS1 females tended to explore less the target quadrant where the platform was previously located than treated APP/PS1 and WT mice, while no differences were observed for the males (Fig. 1I and Fig. S2B). Together, these results suggest that spatial learning might be mildly affected in APP/PS1 females in the absence of treatment, as shown by their poorer discrimination of the target quadrant and thus, weaker retention of the task [47,81].

Following the acquisition phase, mice underwent another set of 4 days in which the platform was relocated to the opposite quadrant, referred to as the reversal phase (days 6–9), to test their cognitive flexibility [53]. Male and female APP/PS1 saline mice exhibited trouble in learning the new position of the platform, as indicated by the significantly higher traveled distance and latency

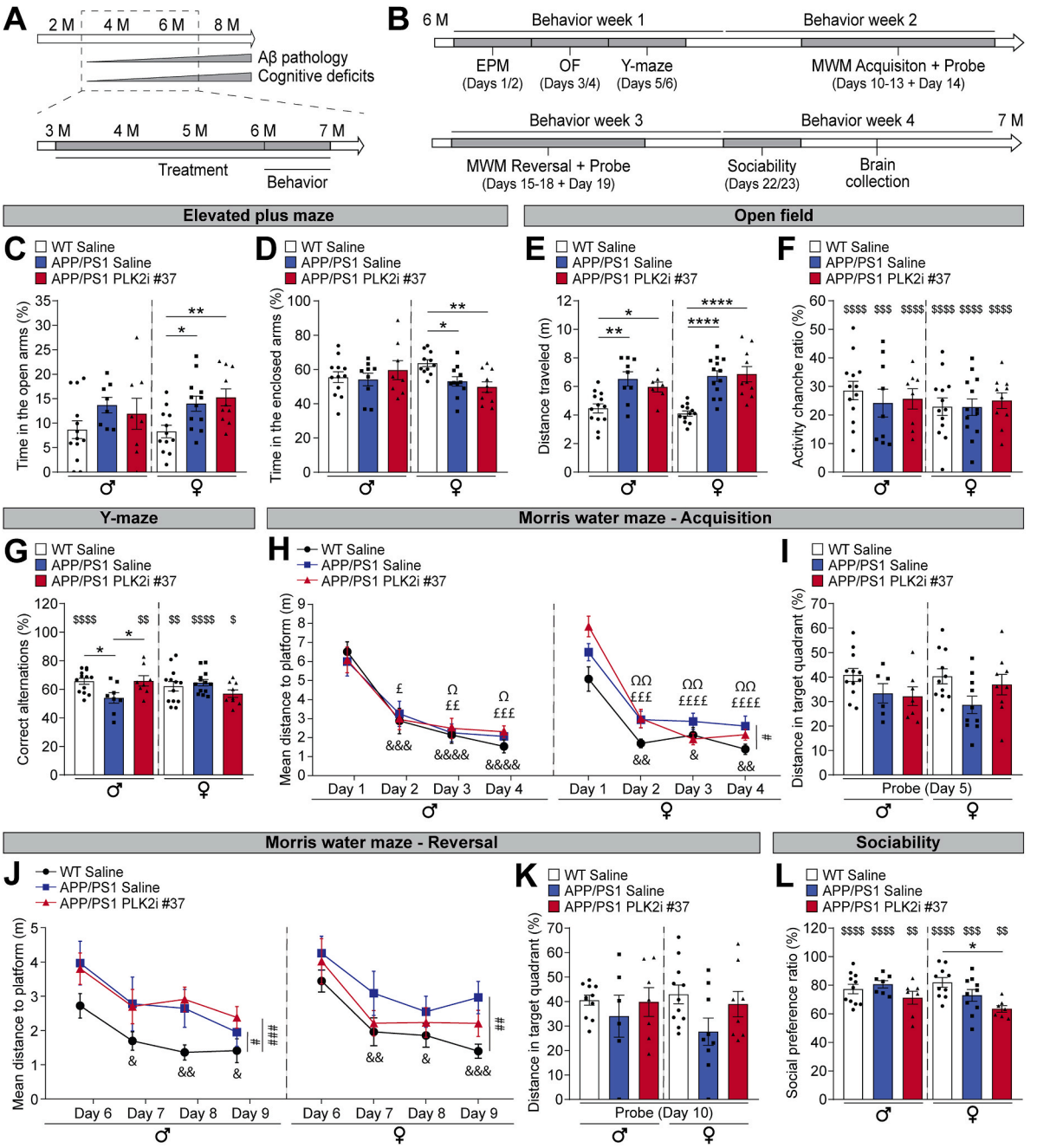

Fig. 1. Chronic treatment with PLK2i #37 reduces cognitive decline in APP/PS1 mice in a sex-dependent manner. (**A**) Temporal line of the experimental design used to evaluate the effect of chronic PLK2 pharmacological inhibition with PLK2i #37 in the APP/PS1 transgenic mouse model of AD. Time represents the age of the mice in months (M). (**B**) Temporal line of the tests used to evaluate behavioral performance in 6- to 7-month-old (±1 week) non-treated WT and non-treated and treated APP/PS1 mice: open field (OF) test, elevated plus maze (EPM) test, Y-maze spontaneous alternation task, Morris water maze (MWM) task, and social approach test (sociability). (**C, D**) Percentage of time spent in (C) the open arms and (D) the enclosed arms during the EPM test. (**E**) Distance traveled in the arena during the first 10 min of the OF test. (**F**) Percentage of activity change (habituation ratio) in the distance traveled between the first 5 min and the last 5 min of the OF test. (**G**) Percentage of correct alternations in the Y-maze spontaneous alternation task. (**H**) Learning curve of the mean distance traveled to reach the platform per day (4 trials per day) during the acquisition phase of the MWM task (days 1–4). (**I**) Percentage of distance traveled in the target quadrant during the post-acquisition probe trial (day 5). (**J**) Learning curve of the mean distance traveled to reach the platform per day (4 trials per day) during the reversal phase of the MWM task (days 6–9). (**K**) Percentage of distance traveled in the target quadrant during the post-reversal probe trial (day 10). (**L**) Percentage of social interaction (social preference ratio) in the three-compartment social approach test. Data are expressed as the group mean ± S.E.M. WT Saline, white (n = 13 per sex); APP/PS1 Saline, blue (n = 9–13 per sex); APP/PS1 PLK2i #37, red (n = 8–10 per sex). One-way ANOVA followed by Tukey's multiple comparisons test (B-F, H, J and K); *$p < 0.05$, **$p < 0.01$, ***$p < 0.001$, ****$p < 0.0001$. One-sample *t*-test (% ≠ 50) (C, F and K); \$ $p < 0.05$, \$\$ $p <$

0.01, $$$ $p < 0.001$, $$$$ $p < 0.0001$. Two-way repeated measures ANOVA followed by Tukey's multiple comparison (differences between groups over time) (G and I); #$p < 0.05$, ##$p < 0.01$, ###$p < 0.001$. Two-way repeated measures ANOVA followed by Dunnett's multiple comparison (versus day 1 for (G) and versus day 6 for (I)); & $p < 0.05$, && $p < 0.01$, &&& $p < 0.001$, &&&& $p < 0.0001$ for WT Saline group; Ω $p < 0.05$, ΩΩ $p < 0.01$ for APP/PS1 Saline; £ $p < 0.05$, ££ $p < 0.01$, £££ $p < 0.001$, ££££ $p < 0.0001$ for APP/PS1 PLK2i #37. (For interpretation of the references to color in this figure legend, the reader is referred to the Web version of this article.)

Table 2
Statistical analysis of sex differences at the behavioral level.

		Two-way ANOVA	Sidak's multiple comparisons test (Males versus females)		
		Effect of sex	WT Saline	APP/PS1 Saline	APP/PS1 PLK2i #37
Elevated plus maze	Time in the open arms	F (1, 57) = 0.5048 p = 0.4803	p = 0.9978	p = 0.9994	p = 0.5581
	Time in the enclosed arms	F (1, 56) = 0.3372 p = 0.5638	p = 0.4661	p = 0.9951	p = 0.1817
Open field	Distance traveled	F (1, 58) = 0.5959 p = 0.4433	p = 0.8537	p = 0.9762	p = 0.3822
	Activity change ratio	F (1, 60) = 0.8267 p = 0.3669	p = 0.4962	p = 0.9881	p = 0.9992
Y-maze	Correct alternations	F (1, 58) = 0.06300 p = 0.8027	p = 0.7217	**p = 0.0434**	p = 0.1561
Morris water maze	Acquisition - Distance in the target quadrant	F (1, 48) = 0.01591 p = 0.9002	p = 0.9937	p = 0.7633	p = 0.7432
	Reversal - Distance in the target quadrant	F (1, 46) = 0.1521 p = 0.6984	p = 0.9722	p = 0.7928	p = 0.9992
Sociability	Social approach ratio	F (1, 46) = 1.494 p = 0.2279	p = 0.6802	p = 0.3663	p = 0.4325

compared to WT mice, which showed significantly decreased distance over time compared to the first day of reversal (day 6) (Fig. 1J and Fig. S2C). Interestingly, treatment with PLK2i #37 did not prevent these deficits in males, as reflected by the significant differences in the overall performance observed between WT mice and both non-treated and treated APP/PS1 groups (Fig. 1J and Fig. S2C). However, while the two-way ANOVA test revealed no sex-related effects (Table 2), performance of treated APP/PS1 females was not different from WT nor non-treated APP/PS1 mice, both for the distance traveled to reach the platform during the reversal phase (Fig. 1J) and the time and distance spent in the target quadrant in the post-reversal probe trials (day 10) (Fig. 1K and Fig. S1D), suggesting an amelioration in their cognitive flexibility.

Finally, the mice's preference for social interaction was measured using the three-compartment social approach test [57–59]. All groups spent more time exploring the social container rather than the empty container (social preference ratio >50 %) (Fig. 1L), indicating good sociability levels. Nevertheless, treated APP/PS1 females were less social than WT counterparts (Fig. 1L), suggesting a potential off-target effect of the treatment in this behavioral aspect. Of note, two-way ANOVA test revealed no effect of sex in this test (Table 2).

Overall, our results suggest that treatment with PLK2i #37 helped in preventing working memory deficits in APP/PS1 males, while slightly improving memory, cognitive flexibility and spatial learning in females.

3.2. *Chronic treatment with PLK2i #37 exacerbates Aβ burden in APP/PS1 mice in a sex-specific manner*

At the cellular level, we first used immunostaining with anti-Aβ 6E10 antibody to assess the number and the size of amyloid plaques in the cortex and dorsal hippocampus of APP/PS1 mice, two parameters commonly used as indicators of the extent of Aβ pathology [5,82,83]. As previously reported [43,60,84], we observed a prominent accumulation of Aβ plaques in the hippocampus and the cortex of APP/PS1 mice (Fig. 2A). This accumulation is more pronounced in female brains [85,86], as reflected by the higher number of plaques (Fig. 2B and D) (Table 3). Interestingly, we observed that treatment with PLK2i #37 further aggravated Aβ pathology, specifically in APP/PS1 females, as reflected by the notable increase in the number of Aβ plaques in the cortex (Fig. 2B) and dorsal hippocampus (Fig. 2D). Of note, the average size of the plaques was not affected by PLK2i #37 treatment (Fig. 2C and E) or by the sex of the animals (Table 3). Together, these results demonstrated that chronic treatment with PLK2i #37 fosters amyloid pathology in female brains, a phenomenon not observed in other transgenic mouse models of AD [23,25].

Next, we evaluated soluble and insoluble Aβ40 and Aβ42 peptide levels in the cortex and hippocampus by ELISA. These two forms of Aβ are particularly relevant because their relative abundance can provide insights into disease pathology and progression [4,87–89]. In line with our immunohistology observations, treatment with PLK2i #37 did not impact the levels of soluble (Fig. 2F and G) or insoluble (Fig. 2H and I) Aβ40 and Aβ42 in the cortex of APP/PS1 males. However, we observed increased cortical Aβ40 (Fig. 2F) and Aβ42 levels (Fig. 2G) in the detergent-soluble fraction in treated APP/PS1 females, compared to non-treated mice. No effects of PLK2 inhibition were detected in the cortical insoluble fraction (guanidine extracts) (Fig. 2H and I). In the hippocampus, no differences between groups were reported for the soluble levels of Aβ40 and Aβ42 (Fig. 2J and K) or the insoluble levels of Aβ42 (Fig. 2M) in either sex. Whereas the levels of insoluble Aβ40 were amplified by the treatment in APP/PS1 females (Fig. 2L). Moreover, soluble, and insoluble Aβ40 and Aβ42 peptide levels differed between males and females in both brain structures (Table 3). Together, these observations show that PLK2i #37 treatment aggravates Aβ pathology and deposition in a sex-specific manner.

To further explore the impact of PLK2 inhibition on Aβ pathology in APP/PS1 mice brains, we used Western blot to evaluate the protein levels of the total and the phosphorylated forms of APP, as well as the APP-derived CTFs, two additional markers of Aβ pathology [22,90,91]. In male APP/PS1 mice, PLK2i #37 treatment induced a decrease in the levels of full-length APP (Fig. 3A and B), as

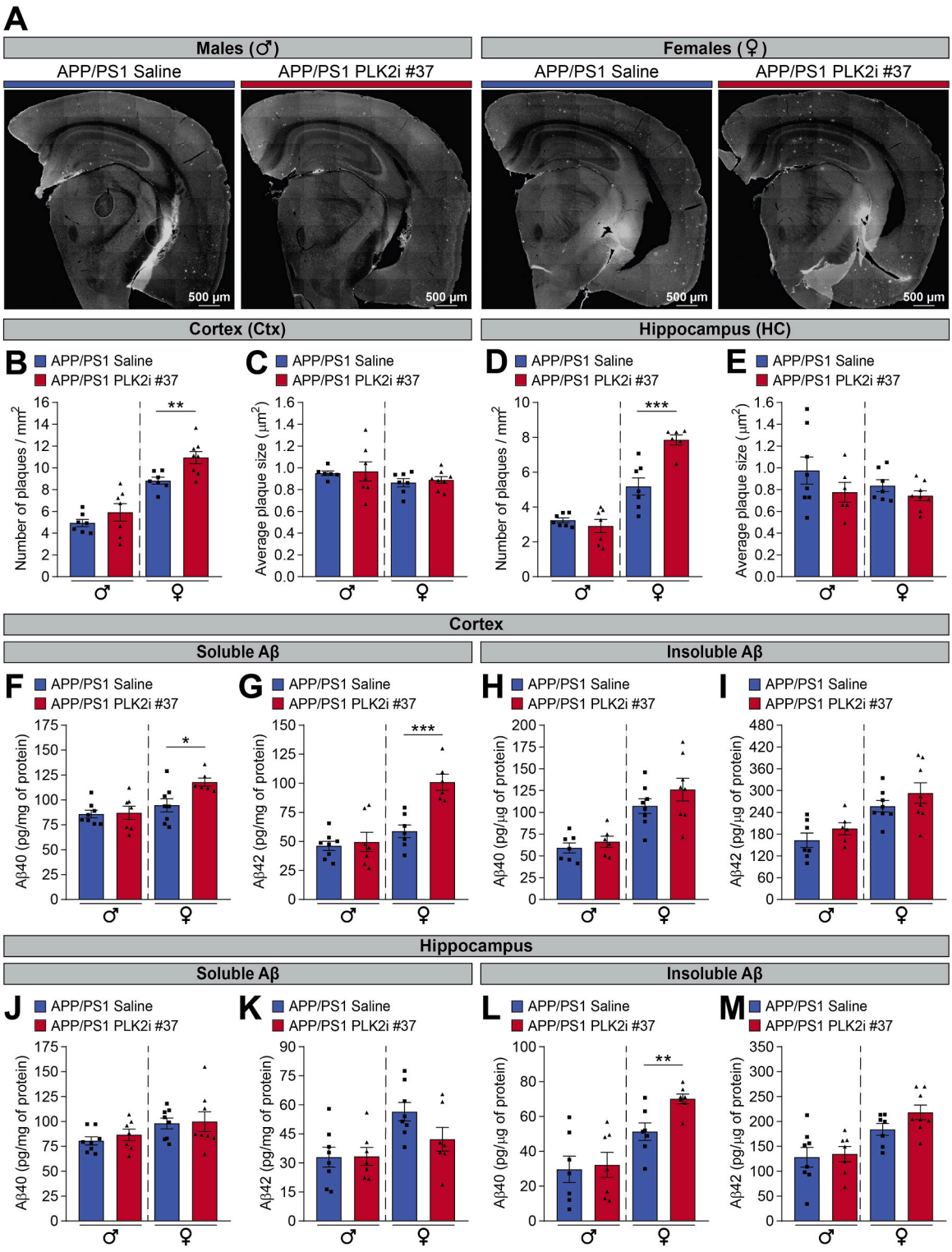

Fig. 2. Chronic treatment with PLK2i #37 increases amyloid plaques and Aβ peptide levels in the cortex and hippocampus of female but not male APP/PS1 mice (**A**) Representative microscopy images of Aβ (6E10) immunofluorescence staining of amyloid plaques in the brain of 7-month-old (±1 week) non-treated and treated APP/PS1 mice. (**B, C**) Quantification of (B) the number of plaques and (C) their average surface in the cortex of non-treated and treated APP/PS1 mice. (**D, E**) Quantification of (D) the number of plaques and (E) their average surface in the dorsal hippocampus of non-treated and treated APP/PS1 mice. (**F-I**) ELISA quantification of the cortical levels of (F, H) Aβ40 and (G, I) Aβ42 peptides in the (F, G) soluble-detergent fraction or (H, I) insoluble fraction (guanidine extracts) of non-treated and treated APP/PS1 mice normalized to total protein. (**J-M**) ELISA

quantification of the hippocampal levels of (J, L) Aβ40 and (K, M) Aβ42 peptides in the (J, K) soluble-detergent fraction or (L, M) insoluble fraction (guanidine extracts) of non-treated and treated APP/PS1 mice normalized to total protein. Data are expressed as the mean group ± S.E.M. APP/PS1 Saline, blue (n = 8 per sex); APP/PS1 PLK2i #37, red (n = 7–8 per sex). Unpaired student t-tests; *$p < 0.05$, **$p < 0.01$, ***$p < 0.001$, ***$p < 0.0001$. (For interpretation of the references to color in this figure legend, the reader is referred to the Web version of this article.)

Table 3
Statistical analysis of sex differences in Aβ pathology.

		Two-way ANOVA	Sidak's multiple comparisons test (Males versus females)	
		Effect of sex	APP/PS1 Saline	APP/PS1 PLK2i #37
Number of plaques	Cortex	F (1, 25) = 66.29 **p < 0.0001**	**p < 0.0001**	**p < 0.0001**
	Hippocampus	F (1, 23) = 93.36 **p < 0.0001**	**p = 0.0013**	**p < 0.0001**
Average plaque size	Cortex	F (1, 24) = 2.559 p = 0.1227	p = 0.4588	p = 0.4725
	Hippocampus	F (1, 25) = 0.9647 p = 0.3354	p = 0.4512	p = 0.9606
Soluble Aβ40 levels	Cortex	F (1, 25) = 12.49 **p = 0.0016**	p = 0.4428	**p = 0.0021**
	Hippocampus	F (1, 27) = 5.173 **p = 0.0311**	p = 0.1416	p = 0.3343
Soluble Aβ42 levels	Cortex	F (1, 24) = 26.22 **p < 0.0001**	p = 0.285	**p < 0.0001**
	Hippocampus	F (1, 26) = 9.780 **p = 0.0043**	**p = 0.0052**	0.4418
Insoluble Aβ40 levels	Cortex	F (1, 25) = 32.26 **p < 0.0001**	**p = 0.0024**	**p = 0.0004**
	Hippocampus	F (1, 24) = 24.83 **p < 0.0001**	**p = 0.0341**	**p = 0.0003**
Insoluble Aβ42 levels	Cortex	F (1, 25) = 19.51 **p = 0.0002**	**p = 0.009**	**p = 0.0089**
	Hippocampus	F (1, 26) = 19.13 **p = 0.0002**	**p = 0.0402**	**p = 0.002**

well as α- and β-CTFs (Fig. 3A, C and D) in the cortex. On the contrary, the treatment increased cortical levels of APP (Fig. 3A and B) and β-CTF (Fig. 3A and C) in APP/PS1 females, without affecting α-CTFs expression levels (Fig. 3A and D). These results support our observation of the sex-dependent increase of amyloid burden in this model upon PLK2 inhibition. In the hippocampus, we did not notice significant effects of the treatment on human APP or β-CTFs levels in APP/PS1 males or females (Fig. 3F–H). However, we did observe a selective reduction in the hippocampal levels of α-CTF, in female, but not in male APP/PS1 mice (Fig. 3F and I). Of note, Western blot analysis showed similar levels of phosphorylated APP at T668 in treated and non-treated groups in the cortex (Fig. 3A and E) and hippocampus (Fig. 3F and J), suggesting that PLK2 may not be the primary kinase catalyzing APP phosphorylation at T668 *in vivo*.

Altogether, these findings demonstrate that chronic PLK2i #37 treatment exacerbates Aβ accumulation and deposition, specifically in female but not male APP/PS1 mice, probably through enhancing APP amyloidogenic processing.

3.3. Chronic treatment with PLK2i #37 does not affect synaptic content in APP/PS1 mice

Our previous work revealed that treatment with PLK2 inhibitor improved synaptic markers in 3xTg-AD mice [23]. These synaptic markers, when reduced, reflect a synaptic dysfunction, a common neuropathological feature of AD [89,92–99]. To investigate whether treatment with PLK2i #37 has also an impact on synaptic pathology in APP/PS1 mice, we used Western blot to analyze the levels of different synaptic proteins, including the pre-synaptic marker Synaptophysin [95], the post-synaptic density protein 95 (PSD95) [94] and Drebrin, present at both the pre- and post-synaptic levels [100]. Our data revealed that the levels of these synaptic proteins in the cortical and hippocampal tissue of APP/PS1 mice remain largely unaffected when compared to WT littermates (Fig. 4A–C and E-G), except for synaptophysin, for which hippocampal and cortical levels were significantly reduced in male and female brains (Fig. 4A, D, E and H). Interestingly, PLK2i #37 treatment did not affect the levels of the three synaptic markers, neither in males nor females (Fig. 4A–H). Unlike our previous study reporting a treatment-induced increase of synaptic marker levels in 3xTg-AD males [23], the present results suggest that chronic treatment with PLK2i #37 does not improve synaptic content in APP/PS1 mice. Moreover, we did not note a sex-dependent effect of the genotype or the treatment for this pathological feature.

4. Discussion

Over the past decades, abnormal protein phosphorylation has emerged as a viable modulable target for the treatment of AD and related dementia [21,22,101–103]. Accumulating evidence place PLK2, a member of a cell-cycle serine/threonine kinase family, among the potential kinases responsible for such imbalance and contributing to AD pathogenesis [23–27]. This suggests that pharmacologically targeting its activity may represent a viable therapeutic strategy for AD and related disorders [23–27]. The present study provides evidence that chronic treatment with PLK2i #37 partially prevented cognitive decline in APP/PS1 mice, in a task- and sex-specific manner. At the cellular level, we observed that the treatment aggravated Aβ accumulation and deposition specifically in female APP/PS1 mice, probably by enhancing APP amyloidogenic processing. Together, our findings demonstrate that PLK2 pharmacological inhibition might have the potential to alleviate cognitive symptoms, but paradoxically exacerbates Aβ pathology in a sex-dependent manner.

At the behavioral level, we observed that chronic PLK2i #37 treatment reduced spatial working memory deficits in male APP/PS1 mice and partially improved female cognitive flexibility-dependent spatial learning and memory. This beneficial effect on the cognitive

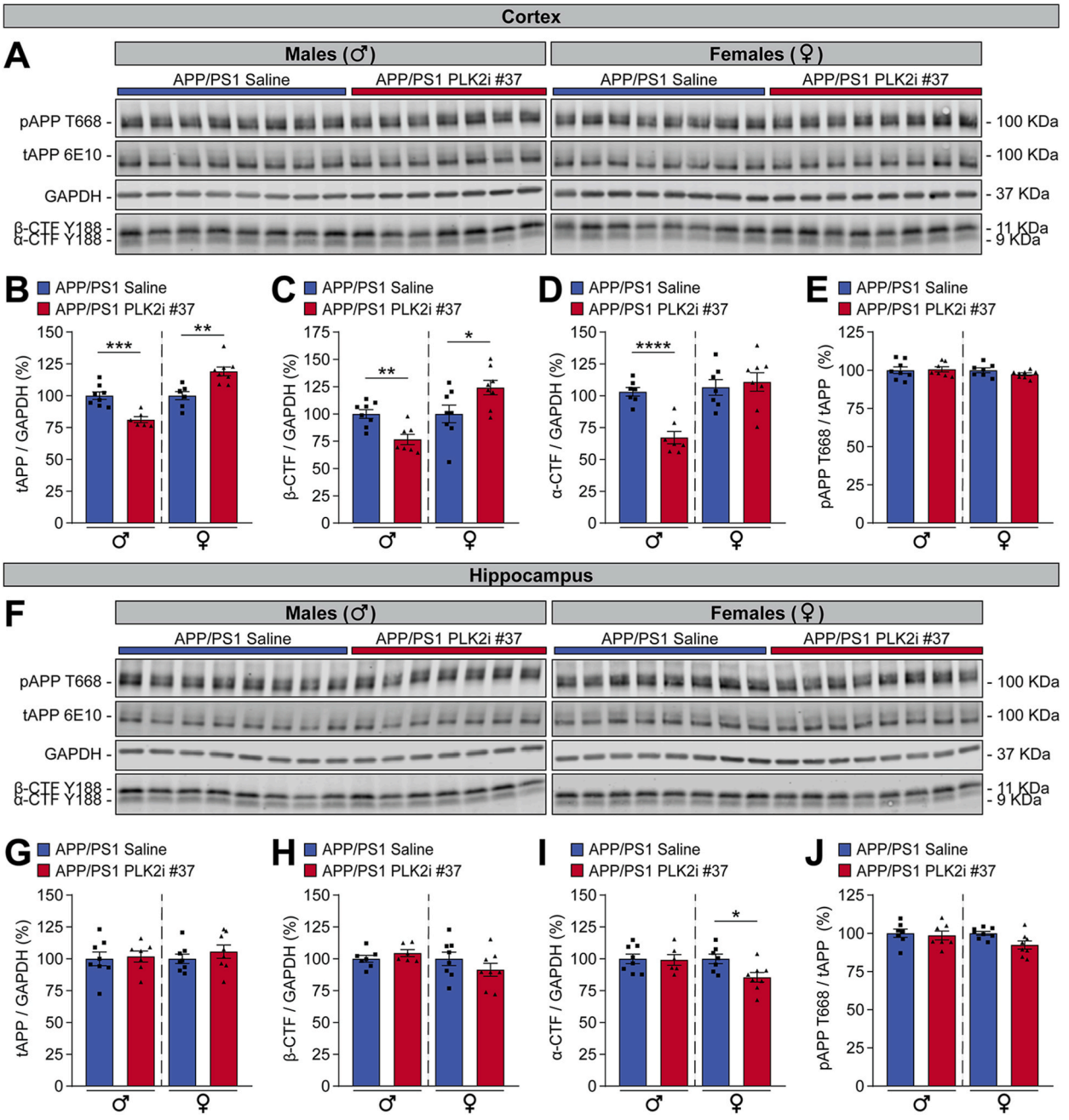

Fig. 3. Chronic treatment with PLK2i #37 affects APP protein expression levels and amyloidogenic processing in APP/PS1 mice in a sex-dependent manner without affecting T668 phosphorylation. (**A**) Western blot analysis of phosphorylated APP (pAPP) T668, full-length human APP (tAPP) (6E10), APP β- and α-CTFs (Y188), and GAPDH in the cortex of 7-month-old (±1 week) non-treated and treated APP/PS1 mice. (**B-D**) Quantification of cortical protein levels of (B) tAPP, (C) β-CTF, and (D) α-CTF expressed as APP/GAPDH percentage normalized to APP/PS1 Saline group. (**E**) Quantification of cortical protein levels of pAPP T668 expressed as pAPP/tAPP percentage normalized to APP/PS1 Saline group. (**F**) Western blot analysis of phosphorylated APP (pAPP) T668, full-length human APP (tAPP) (6E10), APP β- and α-CTFs (Y188), and GAPDH in the hippocampus of 7-month-old (±1 week) non-treated and treated APP/PS1 mice. (**G-J**) Quantification of hippocampal protein levels of (G) tAPP, (H) β-CTF, and (I) α-CTF expressed as APP/GAPDH percentage normalized to APP/PS1 Saline group. (**J**) Quantification of hippocampal protein levels of pAPP T668 expressed as pAPP/tAPP percentage normalized to APP/PS1 Saline group. Data are expressed as the group mean ± S.E.M. APP/PS1 Saline, blue (n = 8 per sex); APP/PS1 PLK2i #37, red (n = 7–8 per sex). Unpaired student t-tests; $*p < 0.05$, $**p < 0.01$, $***p < 0.001$, $***p < 0.0001$. Uncropped original scan images for Western blot membranes are available in Fig. S3. (For interpretation of the references to color in this figure legend, the reader is referred to the Web version of this article.)

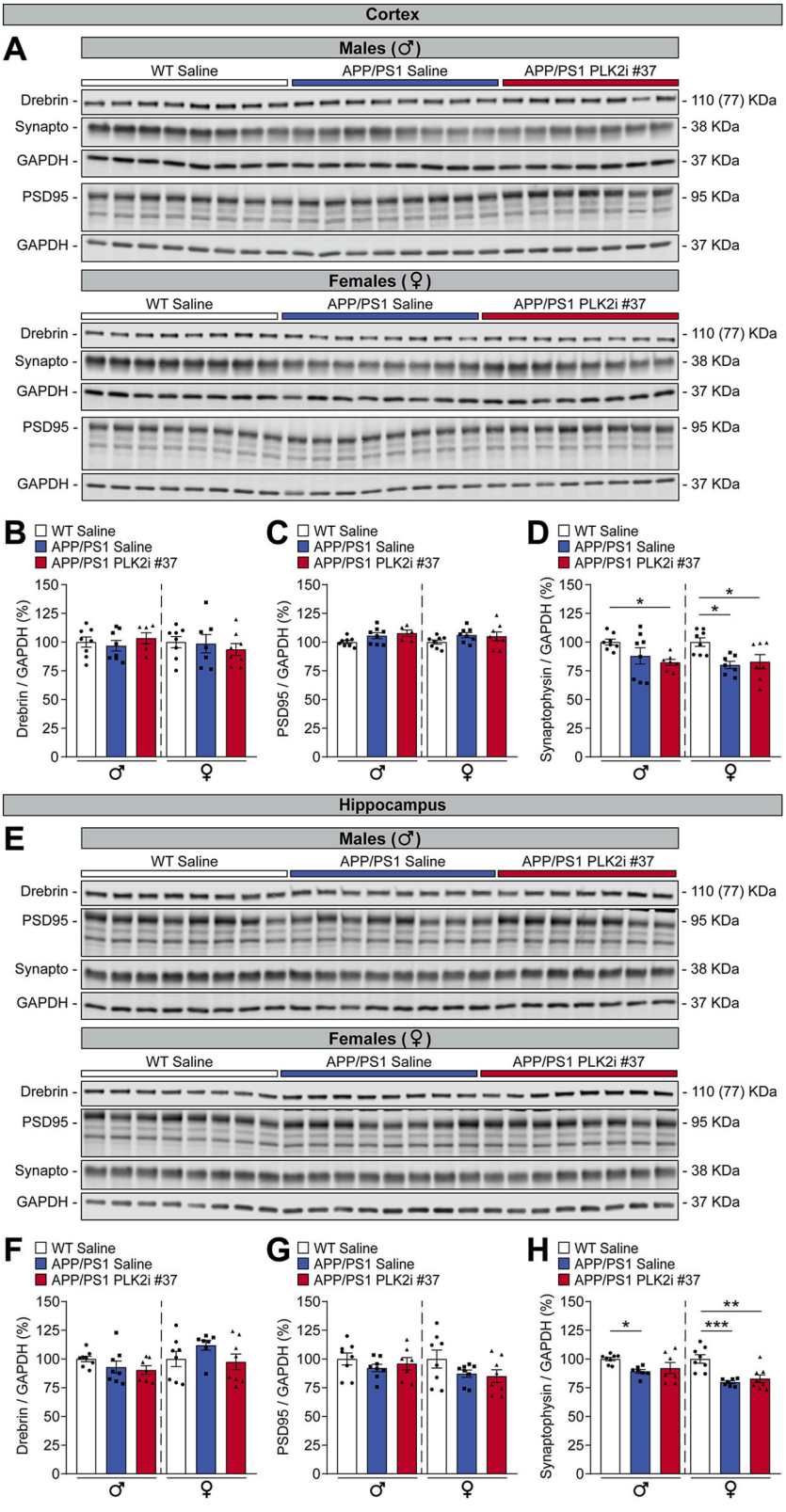

(caption on next page)

Fig. 4. Chronic treatment with PLK2i #37 does not affect synaptic protein levels in APP/PS1 mice. (**A**) Western blot analysis of Drebrin, PSD95, Synaptophysin (Synapto), and GAPDH in the cortex of 7-month-old (±1 week) non-treated WT, and non-treated and treated APP/PS1 mice. (**B-D**) Quantification of cortical protein levels of (B) Drebrin, (C) PDS95, and (D) Synaptophysin expressed as synaptic marker/GAPDH percentage normalized to WT Saline group. (**E**) Western blot analysis of Drebrin, PSD95, Synaptophysin (Synapto), and GAPDH in the hippocampus of 7-month-old (±1 week) non-treated WT, and non-treated and treated APP/PS1 mice. (**F-H**) Quantification of hippocampal protein levels of (F) Drebrin, (G) PDS95, and (H) Synaptophysin expressed as synaptic marker/GAPDH percentage normalized to WT Saline group. Data are expressed as the group mean ± S.E.M. WT Saline, white (n = 8 per sex); APP/PS1 Saline, blue (n = 8 per sex); APP/PS1 PLK2i #37, red (n = 7–8 per sex). One-way ANOVA followed by Tukey's multiple comparisons test; *p < 0.05, **$p < 0.01$, ***$p < 0.001$, ***$p < 0.0001$. Uncropped original scan images for Western blot membranes are available in Fig. S3. (For interpretation of the references to color in this figure legend, the reader is referred to the Web version of this article.)

symptoms is in line with previous studies from our laboratory and others, reporting the rescue of recognition memory deficits in 3xTg-AD and 5XFAD mice, respectively, as well as a reduction of cognitive flexibility impairment in 3xTg-AD mice upon pharmacological inhibition of PLK2 [23,25].

Intriguingly, at the cellular level, PLK2 pharmacological inhibition seems to have variable -and even opposite-effects on Aβ accumulation depending on the animals' genotype and sex. One of the most striking changes reported in the brains of treated APP/PS1 female mice was the increase in the number of amyloid plaques and Aβ peptide levels. In contrast, as we previously reported, transient treatment with PLK2i #37 led to a lower plaque burden in 3xTg-AD females [23]. In males, Aβ pathology remained unchanged by the treatment in both APP/PS1 and 3xTg-AD mouse models [23]. Conversely, in an independent study, the authors reported a reduction in Aβ production and deposition upon genetic or pharmacological inhibition of PLK2 in APP-SwDI and 5XFAD male mice, respectively [25]. While the treatment regimen differed between the studies -and its influence remains to be investigated-, we speculate that additional factors such as the mouse strain, as well as their genetic modifications may also contribute to these differences.

Over the last decades, several studies have demonstrated that genetic background can influence APP processing and Aβ deposition in transgenic mouse models of AD [31–34,104–106]. In addition, a study reported that despite presenting similar Aβ clearance across the blood brain barrier under basal conditions [107,108], various mouse strains commonly used for the development of AD models (C57BL/6, FVB/N, BALB/c, and SJL/J) showed a different response to rifampicin treatment when examining the brain levels of both Aβ clearance and clearance-related proteins [107]. Our results, along with these findings, uphold the hypothesis that the genetic context in which the FAD-mutated transgenes are expressed, have a non-negligible impact on both the resulting AD-associated phenotypes and the effect of pharmacological treatments.

While several research groups have examined the impact of the animals' strain on Aβ pathology specifically, its role in other pathological aspects of the disease remains understudied. Nonetheless, Onos and colleagues reported strain- and sex-specific differences in neurodegeneration upon overexpression of *APPswe* and *PSEN1dE9* transgenes in mice [31]. In line with their findings, our study revealed genotype- and sex-dependent differences in the effect of PLK2 pharmacological inhibition on synaptic pathology, another component of AD [93,99,109]. Here we showed that the treatment did not affect the synaptic content in APP/PS1 mice (harboring *APPswe* and *PSEN1dE9* mutations), whereas we and others had previously observed an increase in synaptic protein levels upon treatment with a PLK2 inhibitor in 3xTg-AD and 5XFAD males, respectively [23,25]. Moreover, neuronal, and synaptic damage are linked to the cognitive deterioration observed in AD [89,95,96,110,111]. Given the impact that genetic variations are postulated to have in the latter [31,32,112,113], our observations could contribute to explain the results obtained at the behavioral level.

In addition to the genetic background of each strain, the differences observed among transgenic mouse models of AD are also strongly dependent on the selected transgenes used to overexpress disease-linked proteins such as APP and Tau. Other factors such as the aggressiveness of the FAD mutations incorporated, as well as the promoter under which the transgenes are expressed, and their number of copies may also play a crucial role [15,20,32,37,112,114,115]. The combination of this myriad of elements results in unique disease-associated phenotypes, age of onset, and progression for each model [35–38]. Thus, the conflicting findings between the present study, our previous results [23], and Lee et al. work [25] regarding the effect of PLK2 pharmacological inhibition may be due, in part, to the use of different AD transgenic lines, namely APP/PS1, 3xTg-AD, and 5XFAD, respectively.

Furthermore, the use of male and female mice in our studies allowed us to investigate the effect of PLK2 pharmacological inhibition on another important AD characteristic, namely sexual dimorphism [116,117]. Our data revealed a strong sex-specific effect of the treatment, both at the behavioral and the cellular levels. Here, we report a prominent exacerbation of Aβ pathology specifically in APP/PS1 females. Similarly, in our previous study, we showed that PLK2i #37 treatment exacerbated Tau pathology in female 3xTg-AD mice, while lowering Tau burden and increasing synaptic protein content in treated males [23]. These findings are of particular relevance, since the sexual dimorphic nature of the disease is also observed in humans, with higher prevalence, worsened pathological features, and faster cognitive decline reported in women [118–123]. Collectively, our findings emphasize the importance of considering sex during both pre-clinical and clinical phases when creating treatments for AD [124].

While the discrepancies observed at the cellular level, especially regarding Aβ pathology, could be attributed to factors such as treatment regimen, animal model, and biological sex. Our results also suggest that the implication of PLK2 in AD might involve mechanisms other than its direct role on APP phosphorylation and processing [23–25]. For instance, PLK2 has been postulated to regulate synaptic homeostasis in the adult brain [125–130] and has been reported to phosphorylate different neuronal targets such as glycogen synthase kinase 3β (GSK-3β), Spine-associated Rap guanosine triphosphatase-activating protein (SPAR), and α-syn [26,41,62,64,125,128]. Thus, we hypothesize that the effects of PLK2 kinase activity and its inhibition on AD pathology might occur at the neuronal level, through the regulation of various cellular processes and signaling pathways, although the exact molecular mechanisms remain to be further investigated. Moreover, the differences observed on the APP levels and its proteolytic derivatives between the

cortex and hippocampus of treated APP/PS1 mice suggest a brain region-dependent effect of the treatment. It is plausible that the expression levels and function of PLK2 and its substrates may vary between brain structures, leading to these differences. Additionally, amyloid plaques and Aβ levels remained unchanged in treated APP/PS1 male mice despite the reported reduction of total APP and β-CTF, suggesting a potential role of PLK2 in other aspects of Aβ pathology such as Aβ degradation and/or clearance [131–134]. Thus, effects of PLK2 pharmacological inhibition through additional targets, whether central or peripheral, such as immune or vascular cells, known to be involved in AD pathology [135–137], cannot be disregarded.

In conclusion, our results highlight the therapeutic capacity of PLK2 inhibition as a treatment for AD, even though its cellular and molecular mechanisms remain elusive. Moreover, our results highlight the importance of sex- and genetic context-dependent differences in studying AD pathophysiology.

They also encourage the need for thorough evaluation and validation of the effects of a potential treatment across different AD models, while taking sex dimorphism into account [23].

CRediT authorship contribution statement

Laura Martínez-Drudis: Writing – review & editing, Writing – original draft, Methodology, Formal analysis, Data curation. **Morgan Bérard:** Methodology, Data curation. **Dylan Musiol:** Conceptualization. **Serge Rivest:** Supervision, Funding acquisition, Formal analysis, Conceptualization. **Abid Oueslati:** Writing – review & editing, Writing – original draft, Validation, Supervision, Project administration, Funding acquisition, Formal analysis, Conceptualization.

Ethics statement

This study was reviewed and approved by the Animal Care Committee of Université Laval with the approval number: 2017108-1, dated September 22, 2017.

Data availability

Data will be made available on request.

Funding statement

This work was supported by the Fondation du CHU de Québec and Alzheimer Society Canada. AO received J1 and J2 salary awards from the FRQS and La Société Parkinson du Québec. SR was supported by a Foundation grant from the Canadian Institutes of Health Research (CIHR).

Declaration of competing interest

The authors declare the following financial interests/personal relationships which may be considered as potential competing interests:Abid Oueslati reports financial support was provided by Quebec Health Research Fund. Abid Oueslati reports financial support was provided by Alzheimer Society of Canada. Serge Rivest reports financial support was provided by Canadian Institutes of Health Research. If there are other authors, they declare that they have no known competing financial interests or personal relationships that could have appeared to influence the work reported in this paper.

Acknowledgements

The graphical abstract was created in BioRender. Oueslati, A. (2024) BioRender.com/n12o726.

Abbreviations

α-syn	α-synuclein
Aβ	Amyloid β
AD	Alzheimer's disease
APP	Amyloid precursor protein
CTF	C-terminal fragment
EPM	Elevated plus maze
FAD	familial Alzheimer's disease
GAPDH	Glyceraldehyde 3-phosphate dehydrogenase
MWM	Morris water maze
OF	Open field
PLK2i #37	PLK2 inhibitor compound #37
PLK2	Polo-like kinase 2
PSD95	Post-synaptic density protein 95

PS/PSEN	Presenilin
PTM	post-translational modification
pS129	phosphorylated α-synuclein at S129
WT	wild-type
3xTg-AD	Triple transgenic mouse model of AD

Appendix A. Supplementary data

Supplementary data to this article can be found online at https://doi.org/10.1016/j.heliyon.2024.e39571.

References

[1] P. Scheltens, et al., Alzheimer's disease, Lancet 397 (10284) (2021) 1577–1590.
[2] S. Long, C. Benoist, W. Weidner, World Alzheimer Report 2023: Reducing Dementia Risk: Never Too Early, Never Too Late, Alzheimer's Disease International, London, England, 2023.
[3] H. Hampel, et al., The amyloid-beta pathway in Alzheimer's disease, Mol. Psychiatr. 26 (10) (2021) 5481–5503.
[4] C.R. Jack Jr., et al., NIA-AA Research Framework: toward a biological definition of Alzheimer's disease, Alzheimers Dement 14 (4) (2018) 535–562.
[5] J. Hardy, D. Allsop, Amyloid deposition as the central event in the aetiology of Alzheimer's disease, Trends Pharmacol. Sci. 12 (10) (1991) 383–388.
[6] J.M. Long, D.M. Holtzman, Alzheimer disease: an update on pathobiology and treatment strategies, Cell 179 (2) (2019) 312–339.
[7] J. Kang, et al., The precursor of Alzheimer's disease amyloid A4 protein resembles a cell-surface receptor, Nature 325 (6106) (1987) 733–736.
[8] D.J. Selkoe, The molecular pathology of Alzheimer's disease, Neuron 6 (4) (1991) 487–498.
[9] X. Xiao, et al., APP, PSEN1, and PSEN2 variants in Alzheimer's disease: systematic Re-evaluation according to ACMG guidelines, Front. Aging Neurosci. 13 (2021) 695808.
[10] E. Bagyinszky, et al., The genetics of Alzheimer's disease, Clin. Interv. Aging 9 (2014) 535–551.
[11] M. Mullan, et al., A pathogenic mutation for probable Alzheimer's disease in the APP gene at the N-terminus of beta-amyloid, Nat. Genet. 1 (5) (1992) 345–347.
[12] R. Crook, et al., A variant of Alzheimer's disease with spastic paraparesis and unusual plaques due to deletion of exon 9 of presenilin 1, Nat. Med. 4 (4) (1998) 452–455.
[13] R. Cacace, K. Sleegers, C. Van Broeckhoven, Molecular genetics of early-onset Alzheimer's disease revisited, Alzheimers Dement 12 (6) (2016) 733–748.
[14] S.J. Webster, et al., Using mice to model Alzheimer's dementia: an overview of the clinical disease and the preclinical behavioral changes in 10 mouse models, Front. Genet. 5 (2014) 88.
[15] G. Esquerda-Canals, et al., Mouse models of Alzheimer's disease, J. Alzheimers Dis. 57 (4) (2017) 1171–1183.
[16] A. Bilkei-Gorzo, Genetic mouse models of brain ageing and Alzheimer's disease, Pharmacol. Ther. 142 (2) (2014) 244–257.
[17] E. Baerends, et al., Modeling the early stages of Alzheimer's disease by administering intracerebroventricular injections of human native Abeta oligomers to rats, Acta Neuropathol. Commun. 10 (1) (2022) 113.
[18] L. Borgstedt, et al., Neurotoxicity of different amyloid beta subspecies in mice and their interaction with isoflurane anaesthesia, PLoS One 15 (12) (2020) e0242989.
[19] D. Puzzo, et al., Rodent models for Alzheimer's disease drug discovery, Expet Opin. Drug Discov. 10 (7) (2015) 703–711.
[20] E. Drummond, T. Wisniewski, Alzheimer's disease: experimental models and reality, Acta Neuropathol. 133 (2) (2017) 155–175.
[21] J. Oliveira, et al., Protein phosphorylation is a key mechanism in Alzheimer's disease, J. Alzheimers Dis. 58 (4) (2017) 953–978.
[22] T. Zhang, D. Chen, T.H. Lee, Phosphorylation signaling in APP processing in Alzheimer's disease, Int. J. Mol. Sci. 21 (1) (2019).
[23] L. Martinez-Drudis, et al., Inhibition of PLK2 activity affects APP and tau pathology and improves synaptic content in a sex-dependent manner in a 3xTg mouse model of Alzheimer's disease, Neurobiol. Dis. 172 (2022) 105833.
[24] Y. Lee, et al., Polo-like kinase 2 phosphorylation of amyloid precursor protein regulates activity-dependent amyloidogenic processing, Neuropharmacology 117 (2017) 387–400.
[25] J.S. Lee, et al., Inhibition of Polo-like kinase 2 ameliorates pathogenesis in Alzheimer's disease model mice, PLoS One 14 (7) (2019) e0219691.
[26] M.K. Mbefo, et al., Phosphorylation of synucleins by members of the Polo-like kinase family, J. Biol. Chem. 285 (4) (2010) 2807–2822.
[27] P.L. Harris, et al., Neuronal polo-like kinase in Alzheimer disease indicates cell cycle changes, Neurobiol. Aging 21 (6) (2000) 837–841.
[28] E. Bufill, et al., Reelin signaling pathway genotypes and Alzheimer disease in a Spanish population, Alzheimer Dis. Assoc. Disord. 29 (2) (2015) 169–172.
[29] S. Oddo, et al., Amyloid deposition precedes tangle formation in a triple transgenic model of Alzheimer's disease, Neurobiol. Aging 24 (8) (2003) 1063–1070.
[30] S. Oddo, et al., Triple-transgenic model of Alzheimer's disease with plaques and tangles: intracellular Abeta and synaptic dysfunction, Neuron 39 (3) (2003) 409–421.
[31] K.D. Onos, et al., Enhancing face validity of mouse models of Alzheimer's disease with natural genetic variation, PLoS Genet. 15 (5) (2019) e1008155.
[32] S.M. Neuner, et al., Harnessing genetic complexity to enhance translatability of Alzheimer's disease mouse models: a path toward precision medicine, Neuron 101 (3) (2019) 399–411 e5.
[33] D. Ryman, B.T. Lamb, Genetic and environmental modifiers of Alzheimer's disease phenotypes in the mouse, Curr. Alzheimer Res. 3 (5) (2006) 465–473.
[34] E.J. Lehman, et al., Genetic background regulates beta-amyloid precursor protein processing and beta-amyloid deposition in the mouse, Hum. Mol. Genet. 12 (22) (2003) 2949–2956.
[35] G.A. Elder, M.A. Gama Sosa, R. De Gasperi, Transgenic mouse models of Alzheimer's disease, Mt. Sinai J. Med. 77 (1) (2010) 69–81.
[36] M. Yokoyama, et al., Mouse models of Alzheimer's disease, Front. Mol. Neurosci. 15 (2022) 912995.
[37] R. Sanchez-Varo, et al., Transgenic mouse models of Alzheimer's disease: an integrative analysis, Int. J. Mol. Sci. 23 (10) (2022).
[38] K.E. Ameen-Ali, et al., Review: neuropathology and behavioural features of transgenic murine models of Alzheimer's disease, Neuropathol. Appl. Neurobiol. 43 (7) (2017) 553–570.
[39] S. Bowers, et al., Design and synthesis of highly selective, orally active Polo-like kinase-2 (Plk-2) inhibitors, Bioorg. Med. Chem. Lett. 23 (9) (2013) 2743–2749.
[40] R.H. Kofoed, et al., Polo-like kinase 2 modulates alpha-synuclein protein levels by regulating its mRNA production, Neurobiol. Dis. 106 (2017) 49–62.
[41] S. Elfarrash, et al., Polo-like kinase 2 inhibition reduces serine-129 phosphorylation of physiological nuclear alpha-synuclein but not of the aggregated alpha-synuclein, PLoS One 16 (10) (2021) e0252635.
[42] J.L. Jankowsky, et al., Co-expression of multiple transgenes in mouse CNS: a comparison of strategies, Biomol. Eng. 17 (6) (2001) 157–165.
[43] M. Garcia-Alloza, et al., Characterization of amyloid deposition in the APPswe/PS1dE9 mouse model of Alzheimer disease, Neurobiol. Dis. 24 (3) (2006) 516–524.
[44] A.A. Walf, C.A. Frye, The use of the elevated plus maze as an assay of anxiety-related behavior in rodents, Nat. Protoc. 2 (2) (2007) 322–328.
[45] R.G. Lister, The use of a plus-maze to measure anxiety in the mouse, Psychopharmacology (Berl) 92 (2) (1987) 180–185.

[46] A. Maxan, et al., Use of adeno-associated virus-mediated delivery of mutant huntingtin to study the spreading capacity of the protein in mice and non-human primates, Neurobiol. Dis. 141 (2020) 104951.
[47] J.N. Crawley, Behavioral phenotyping of transgenic and knockout mice: experimental design and evaluation of general health, sensory functions, motor abilities, and specific behavioral tests, Brain Res. 835 (1) (1999) 18–26.
[48] R.N. Walsh, R.A. Cummins, The Open-Field Test: a critical review, Psychol. Bull. 83 (3) (1976) 482–504.
[49] V.J. Bolivar, Intrasession and intersession habituation in mice: from inbred strain variability to linkage analysis, Neurobiol. Learn. Mem. 92 (2) (2009) 206–214.
[50] R. Lalonde, The neurobiological basis of spontaneous alternation, Neurosci. Biobehav. Rev. 26 (1) (2002) 91–104.
[51] A.K. Kraeuter, P.C. Guest, Z. Sarnyai, The Y-maze for assessment of spatial working and reference memory in mice, Methods Mol. Biol. 1916 (2019) 105–111.
[52] M. Alpaugh, et al., Passive immunization against phosphorylated tau improves features of Huntington's disease pathology, Mol. Ther. 30 (4) (2022) 1500–1522.
[53] C.V. Vorhees, M.T. Williams, Morris water maze: procedures for assessing spatial and related forms of learning and memory, Nat. Protoc. 1 (2) (2006) 848–858.
[54] R.G.M. Morris, Spatial localization does not require the presence of local cues, Learn. Motiv. 12 (2) (1981) 239–260.
[55] R. Morris, Developments of a water-maze procedure for studying spatial learning in the rat, J. Neurosci. Methods 11 (1) (1984) 47–60.
[56] M. Berard, et al., Non-invasive systemic viral delivery of human alpha-synuclein mimics selective and progressive neuropathology of Parkinson's disease in rodent brains, Mol. Neurodegener. 18 (1) (2023) 91.
[57] J.J. Nadler, et al., Automated apparatus for quantitation of social approach behaviors in mice, Gene Brain Behav. 3 (5) (2004) 303–314.
[58] S.S. Moy, et al., Sociability and preference for social novelty in five inbred strains: an approach to assess autistic-like behavior in mice, Gene Brain Behav. 3 (5) (2004) 287–302.
[59] J.N. Crawley, Mouse behavioral assays relevant to the symptoms of autism, Brain Pathol. 17 (4) (2007) 448–459.
[60] M.N. Gordon, et al., Time course of the development of Alzheimer-like pathology in the doubly transgenic PS1+APP mouse, Exp. Neurol. 173 (2) (2002) 183–195.
[61] K.J. Inglis, et al., Polo-like kinase 2 (PLK2) phosphorylates alpha-synuclein at serine 129 in central nervous system, J. Biol. Chem. 284 (5) (2009) 2598–2602.
[62] A. Oueslati, et al., Polo-like kinase 2 regulates selective autophagic alpha-synuclein clearance and suppresses its toxicity in vivo, Proc. Natl. Acad. Sci. U. S. A. 110 (41) (2013) E3945–E3954.
[63] B.D. Looyenga, P. Brundin, Silencing synuclein at the synapse with PLK2, Proc. Natl. Acad. Sci. U. S. A. 110 (41) (2013) 16293–16294.
[64] M. Dahmene, M. Berard, A. Oueslati, Dissecting the molecular pathway involved in PLK2 kinase-mediated alpha-Synuclein-selective autophagic degradation, J. Biol. Chem. 292 (9) (2017) 3919–3928.
[65] L.J. Weston, et al., Genetic deletion of Polo-like kinase 2 reduces alpha-synuclein serine-129 phosphorylation in presynaptic terminals but not Lewy bodies, J. Biol. Chem. 296 (2021) 100273.
[66] N. Ramalingam, et al., Dynamic physiological alpha-synuclein S129 phosphorylation is driven by neuronal activity, NPJ Parkinsons Dis 9 (1) (2023) 4.
[67] M.L. Seibenhener, M.C. Wooten, Use of the Open Field Maze to measure locomotor and anxiety-like behavior in mice, J. Vis. Exp. (96) (2015) e52434.
[68] S.P. Rodgers, et al., Transgenic APP expression during postnatal development causes persistent locomotor hyperactivity in the adult, Mol. Neurodegener. 7 (2012) 28.
[69] H. Huang, et al., Characterization of AD-like phenotype in aged APPSwe/PS1dE9 mice, Age (Dordr) 38 (4) (2016) 303–322.
[70] L.A. Hulshof, et al., Both male and female APPswe/PSEN1dE9 mice are impaired in spatial memory and cognitive flexibility at 9 months of age, Neurobiol. Aging 113 (2022) 28–38.
[71] L. Xu, et al., Deficits in N-Methyl-D-Aspartate receptor function and synaptic plasticity in hippocampal CA1 in APP/PS1 mouse model of Alzheimer's disease, Front. Aging Neurosci. 13 (2021) 772980.
[72] D. Jansen, et al., A longitudinal study of cognition, proton MR spectroscopy and synaptic and neuronal pathology in aging wild-type and AbetaPPswe-PS1dE9 mice, PLoS One 8 (5) (2013) e63643.
[73] T. Blackmore, et al., Tracking progressive pathological and functional decline in the rTg4510 mouse model of tauopathy, Alzheimer's Res. Ther. 9 (1) (2017) 77.
[74] E.K. Pickett, et al., Amyloid beta and tau cooperate to cause reversible behavioral and transcriptional deficits in a model of Alzheimer's disease, Cell Rep. 29 (11) (2019) 3592–3604 e5.
[75] R. Migliaccio, et al., Cognitive and behavioural inhibition deficits in neurodegenerative dementias, Cortex 131 (2020) 265–283.
[76] L.I. Mariano, et al., Disinhibition in frontotemporal dementia and Alzheimer's disease: a neuropsychological and behavioural investigation, J. Int. Neuropsychol. Soc. 26 (2) (2020) 163–171.
[77] F.J. Gil-Bea, et al., Increase of locomotor activity underlying the behavioral disinhibition in tg2576 mice, Behav. Neurosci. 121 (2) (2007) 340–344.
[78] R. Lalonde, H.D. Kim, K. Fukuchi, Exploratory activity, anxiety, and motor coordination in bigenic APPswe + PS1/DeltaE9 mice, Neurosci. Lett. 369 (2) (2004) 156–161.
[79] R.S. Reiserer, et al., Impaired spatial learning in the APPSwe + PSEN1DeltaE9 bigenic mouse model of Alzheimer's disease, Gene Brain Behav. 6 (1) (2007) 54–65.
[80] J.J. Gallagher, A.M. Minogue, M.A. Lynch, Impaired performance of female APP/PS1 mice in the Morris water maze is coupled with increased Abeta accumulation and microglial activation, Neurodegener. Dis. 11 (1) (2013) 33–41.
[81] A.L. Hemonnot-Girard, et al., Analysis of CX3CR1 haplodeficiency in male and female APP(swe)/PSEN1(dE9) mice along Alzheimer disease progression, Brain Behav. Immun. 91 (2021) 404–417.
[82] A. Christensen, C.J. Pike, Staining and quantification of beta-amyloid pathology in transgenic mouse models of Alzheimer's disease, Methods Mol. Biol. 2144 (2020) 211–221.
[83] P. Yan, et al., Characterizing the appearance and growth of amyloid plaques in APP/PS1 mice, J. Neurosci. 29 (34) (2009) 10706–10714.
[84] J.L. Jankowsky, et al., Mutant presenilins specifically elevate the levels of the 42 residue beta-amyloid peptide in vivo: evidence for augmentation of a 42-specific gamma secretase, Hum. Mol. Genet. 13 (2) (2004) 159–170.
[85] Y. Ni, et al., Activation of beta2-adrenergic receptor stimulates gamma-secretase activity and accelerates amyloid plaque formation, Nat. Med. 12 (12) (2006) 1390–1396.
[86] S. Lecordier, et al., Multifocal cerebral microinfarcts modulate early Alzheimer's disease pathology in a sex-dependent manner, Front. Immunol. 12 (2021) 813536.
[87] T. Iwatsubo, et al., Visualization of A beta 42(43) and A beta 40 in senile plaques with end-specific A beta monoclonals: evidence that an initially deposited species is A beta 42(43), Neuron 13 (1) (1994) 45–53.
[88] A.M. Foley, et al., Systematic review of the relationship between amyloid-beta levels and measures of transgenic mouse cognitive deficit in Alzheimer's disease, J. Alzheimers Dis. 44 (3) (2015) 787–795.
[89] C. Tremblay, et al., Association of neuropathological markers in the parietal cortex with antemortem cognitive function in persons with mild cognitive impairment and Alzheimer disease, J. Neuropathol. Exp. Neurol. 76 (2) (2017) 70–88.
[90] M.S. Garcia-Ayllon, et al., C-terminal fragments of the amyloid precursor protein in cerebrospinal fluid as potential biomarkers for Alzheimer disease, Sci. Rep. 7 (1) (2017) 2477.
[91] S.E. Lee, et al., Accumulation of APP-CTF induces mitophagy dysfunction in the iNSCs model of Alzheimer's disease, Cell Death Dis. 8 (1) (2022) 1.
[92] G. Kashyap, et al., Synapse loss and progress of Alzheimer's disease -A network model, Sci. Rep. 9 (1) (2019) 6555.
[93] F.M. LaFerla, S. Oddo, Alzheimer's disease: abeta, tau and synaptic dysfunction, Trends Mol. Med. 11 (4) (2005) 170–176.

[94] A. Savioz, G. Leuba, P.G. Vallet, A framework to understand the variations of PSD-95 expression in brain aging and in Alzheimer's disease, Ageing Res. Rev. 18 (2014) 86–94.
[95] C.I. Sze, et al., Loss of the presynaptic vesicle protein synaptophysin in hippocampus correlates with cognitive decline in Alzheimer disease, J. Neuropathol. Exp. Neurol. 56 (8) (1997) 933–944.
[96] C. Tremblay, et al., Biochemical characterization of Abeta and tau pathologies in mild cognitive impairment and Alzheimer's disease, J. Alzheimers Dis. 12 (4) (2007) 377–390.
[97] E. Masliah, et al., Altered expression of synaptic proteins occurs early during progression of Alzheimer's disease, Neurology 56 (1) (2001) 127–129.
[98] K. Hatanpaa, et al., Loss of proteins regulating synaptic plasticity in normal aging of the human brain and in Alzheimer disease, J. Neuropathol. Exp. Neurol. 58 (6) (1999) 637–643.
[99] P.H. Reddy, et al., Differential loss of synaptic proteins in Alzheimer's disease: implications for synaptic dysfunction, J. Alzheimers Dis. 7 (2) (2005) 103–117. ; discussion 173-80.
[100] Y. Ishizuka, K. Hanamura, Drebrin in Alzheimer's disease, Adv. Exp. Med. Biol. 1006 (2017) 203–223.
[101] Z. Li, et al., Targeting protein kinases for the treatment of Alzheimer's disease: recent progress and future perspectives, Eur. J. Med. Chem. 261 (2023) 115817.
[102] F. Fagiani, et al., Targeting dementias through cancer kinases inhibition, Alzheimers Dement (N Y) 6 (1) (2020) e12044.
[103] A.B. Engin, A. Engin, Alzheimer's disease and protein kinases, Adv. Exp. Med. Biol. 1275 (2021) 285–321.
[104] H.M. Jackson, et al., DBA/2J genetic background exacerbates spontaneous lethal seizures but lessens amyloid deposition in a mouse model of Alzheimer's disease, PLoS One 10 (5) (2015) e0125897.
[105] D. Ryman, Y. Gao, B.T. Lamb, Genetic loci modulating amyloid-beta levels in a mouse model of Alzheimer's disease, Neurobiol. Aging 29 (8) (2008) 1190–1198.
[106] J.D. Sipe, et al., Characterization of the inbred CE/J mouse strain as amyloid resistant, Am. J. Pathol. 143 (5) (1993) 1480–1485.
[107] H. Qosa, A. Kaddoumi, Effect of mouse strain as a background for Alzheimer's disease models on the clearance of amyloid-beta, J. Syst. Integr. Neurosci. 2 (2) (2016) 135–140.
[108] H. Qosa, et al., Differences in amyloid-beta clearance across mouse and human blood-brain barrier models: kinetic analysis and mechanistic modeling, Neuropharmacology 79 (2014) 668–678.
[109] J. Griffiths, S.G.N. Grant, Synapse pathology in Alzheimer's disease, Semin. Cell Dev. Biol. 139 (2023) 13–23.
[110] S.T. DeKosky, S.W. Scheff, Synapse loss in frontal cortex biopsies in Alzheimer's disease: correlation with cognitive severity, Ann. Neurol. 27 (5) (1990) 457–464.
[111] R.D. Terry, et al., Physical basis of cognitive alterations in Alzheimer's disease: synapse loss is the major correlate of cognitive impairment, Ann. Neurol. 30 (4) (1991) 572–580.
[112] K.D. Onos, et al., Toward more predictive genetic mouse models of Alzheimer's disease, Brain Res. Bull. 122 (2016) 1–11.
[113] M. Gatz, et al., Heritability for Alzheimer's disease: the study of dementia in Swedish twins, J. Gerontol A Biol. Sci. Med. Sci. 52 (2) (1997) M117–M125.
[114] J.L. Jankowsky, H. Zheng, Practical considerations for choosing a mouse model of Alzheimer's disease, Mol. Neurodegener. 12 (1) (2017) 89.
[115] A.M. Hall, E.D. Roberson, Mouse models of Alzheimer's disease, Brain Res. Bull. 88 (1) (2012) 3–12.
[116] D. Zhu, A. Montagne, Z. Zhao, Alzheimer's pathogenic mechanisms and underlying sex difference, Cell. Mol. Life Sci. 78 (11) (2021) 4907–4920.
[117] C.M. Mazure, J. Swendsen, Sex differences in Alzheimer's disease and other dementias, Lancet Neurol. 15 (5) (2016) 451–452.
[118] D.W. Fisher, D.A. Bennett, H. Dong, Sexual dimorphism in predisposition to Alzheimer's disease, Neurobiol. Aging 70 (2018) 308–324.
[119] M.M. Mielke, P. Vemuri, W.A. Rocca, Clinical epidemiology of Alzheimer's disease: assessing sex and gender differences, Clin. Epidemiol. 6 (2014) 37–48.
[120] J.L. Podcasy, C.N. Epperson, Considering sex and gender in Alzheimer disease and other dementias, Dialogues Clin. Neurosci. 18 (4) (2016) 437–446.
[121] J.A. Luchsinger, et al., Sex differences in in vivo Alzheimer's disease neuropathology in late middle-aged Hispanics, J. Alzheimers Dis. 74 (4) (2020) 1243–1252.
[122] L. Edwards, et al., Multimodal neuroimaging of sex differences in cognitively impaired patients on the Alzheimer's continuum: greater tau-PET retention in females, Neurobiol. Aging 105 (2021) 86–98.
[123] S. Oveisgharan, et al., Sex differences in Alzheimer's disease and common neuropathologies of aging, Acta Neuropathol. 136 (6) (2018) 887–900.
[124] M.A. Lynch, A case for seeking sex-specific treatments in Alzheimer's disease, Front. Aging Neurosci. 16 (2024) 1346621.
[125] K.J. Lee, et al., Requirement for Plk2 in orchestrated ras and rap signaling, homeostatic structural plasticity, and memory, Neuron 69 (5) (2011) 957–973.
[126] A.B. Mihalas, et al., Opposing action of nuclear factor kappaB and Polo-like kinases determines a homeostatic end point for excitatory synaptic adaptation, J. Neurosci. 33 (42) (2013) 16490–16501.
[127] D.M. Evers, et al., Plk2 attachment to NSF induces homeostatic removal of GluA2 during chronic overexcitation, Nat. Neurosci. 13 (10) (2010) 1199–1207.
[128] D.P. Seeburg, et al., Critical role of CDK5 and Polo-like kinase 2 in homeostatic synaptic plasticity during elevated activity, Neuron 58 (4) (2008) 571–583.
[129] D.P. Seeburg, M. Sheng, Activity-induced Polo-like kinase 2 is required for homeostatic plasticity of hippocampal neurons during epileptiform activity, J. Neurosci. 28 (26) (2008) 6583–6591.
[130] X.L. Ang, et al., Regulation of postsynaptic RapGAP SPAR by Polo-like kinase 2 and the SCFbeta-TRCP ubiquitin ligase in hippocampal neurons, J. Biol. Chem. 283 (43) (2008) 29424–29432.
[131] D.J. Selkoe, J. Hardy, The amyloid hypothesis of Alzheimer's disease at 25 years, EMBO Mol. Med. 8 (6) (2016) 595–608.
[132] Y. Zhang, et al., Amyloid beta-based therapy for Alzheimer's disease: challenges, successes and future, Signal Transduct. Targeted Ther. 8 (1) (2023) 248.
[133] G.F. Chen, et al., Amyloid beta: structure, biology and structure-based therapeutic development, Acta Pharmacol. Sin. 38 (9) (2017) 1205–1235.
[134] W. Cai, T. Wu, N. Chen, The amyloid-beta clearance: from molecular targets to glial and neural cells, Biomolecules 13 (2) (2023).
[135] M. Jorfi, A. Maaser-Hecker, R.E. Tanzi, The neuroimmune axis of Alzheimer's disease, Genome Med. 15 (1) (2023) 6.
[136] S. Jevtic, et al., The role of the immune system in Alzheimer disease: etiology and treatment, Ageing Res. Rev. 40 (2017) 84–94.
[137] K. Govindpani, et al., Vascular dysfunction in Alzheimer's disease: a prelude to the pathological process or a consequence of it? J. Clin. Med. 8 (5) (2019).